Journal of Alloys and Compounds 509 (2011) 8825–8831

Contents lists available at ScienceDirect

Journal of Alloys and Compounds

journal homepage: www.elsevier.com/locate/jallcom

Synthesis and characterization of polypropiolate sodium (PPNa)–Fe_3O_4 nanocomposite

S. Bahçeci[a], B. Unal[a,b,c], A. Baykal[a,c,*], H. Sözeri[d], E. Karaoglu[a], B. Esat[a]

[a] Department of Chemistry, Fatih University, 34500, B. Cekmece, Istanbul, Turkey
[b] Department of Electrical & Electronics Engineering, and Fatih University, 34500, B. Cekmece, Istanbul, Turkey
[c] BioNanoTechnology R&D Center, Fatih University, 34500, B. Cekmece, Istanbul, Turkey
[d] TUBITAK-UME, National Metrology Institute, PO Box 54, 41470, Gebze, Kocaeli, Turkey

ARTICLE INFO

Article history:
Received 1 June 2011
Received in revised form 17 June 2011
Accepted 18 June 2011
Available online 24 June 2011

Keywords:
Nanocomposite
Magnetic nanomaterials
Conductivity
Dielectric properties
Polypropiolate

ABSTRACT

Polypropiolate sodium (PPNa)–Fe_3O_4 nanocomposites were successfully synthesized by the precipitation of Fe_3O_4 in the presence of sodium polypropiolate and followed by reflux route. Structural, morphological, electrical and magnetic properties evaluation of the nanocomposite were performed by X-ray powder diffraction (XRD), Fourier transform infrared spectroscopy (FT-IR), transmission electron microscopy (TEM), thermal gravimetric analysis (TGA), vibrating scanning magnetometry (VSM) and conductivity measurements. Crystalline phase was identified as magnetite with an average crystallite size of 7 ± 3 nm as estimated from X-ray line profile fitting. Particle size estimated from TEM, by log-normal fitting, is $\sim 9 \pm 1$ nm. FT-IR analysis shows that the binding of PPNa on the surface of iron oxide is through bidentate linkage of carboxyl group. TGA analysis showed the presence of 20% PPNa around 80% magnetic core (Fe_3O_4). . .PPNa–Fe_3O_4 nanocomposite show superparamagnetic characteristics at room temperature. It is found that the a.c. conductivity of the nanocomposites obeys the well-known power law of frequency in which it also depends on temperature. Additionally, its d.c. conductivity showed that two operating regions of the activation energy. Both real and imaginary parts of either permittivity exhibit almost the same attitudes which are the indication of the same ability in the stored energy, and dissipation of energy within the PPNa and PPNa–Fe_3O_4 nanocomposites.

1. Introduction

Magnetic NPs have many unique magnetic properties such as superparamagnetic, high coercivity, low Curie temperature, high magnetic susceptibility, etc. Magnetic NPs are of great interest for researchers from a broad range of disciplines, including magnetic fluids, data storage, catalysis, and bioapplications [1–6].

Superparamagnetic magnetite (Fe_3O_4) NP's are getting great interest in the past few decades due to their unique chemical and physical properties. Moreover, the naked iron oxide NPs have high chemical activity, and are easily oxidized in air (especially magnetite), generally resulting in loss of magnetism and dispersibility. Therefore, providing proper surface coating and developing some effective protection strategies (to form core/shell structured materials) to keep the stability of magnetic iron oxide NPs is very important. Surfactants act as protecting agent for controlling particle size and stabilizing the colloidal dispersions (polymers coating will increase repulsive forces to balance the magnetic and the van der Waals attractive forces acting on the NP's. Practically, it is worthy that in many cases the protecting shells not only stabilize the magnetic iron oxide NPs, but can also be used for further functionalization [1,7–9]. Moreover, polymer functionalized iron oxide NPs have been extensively investigated due to interest in their unique physical or chemical properties [10].

In the present article, polypropiolate sodium (PPNa)–Fe_3O_4 nanocomposite was successfully synthesized and its chemical–physical properties are evaluated. The size, structure and surface properties of polypropiolate sodium (PPNa)–Fe_3O_4 nanocomposite were studied with transmission electron microscopy (TEM), X-ray diffraction (XRD), and Fourier transform infrared (FT-IR) spectroscopy respectively. Magnetic and conductivity properties were characterized by vibrating sample magnetometer (VSM) and conductivity measurements. And also detailed electrical properties of the (PPNa)–Fe_3O_4 nanocomposite were also presented first time in this study.

* Corresponding author at: Department of Chemistry, Fatih University, 34500, B. Cekmece, Istanbul, Turkey.
E-mail address: hbaykal@fatih.edu.tr (A. Baykal).

0925-8388/$ – see front matter © 2011 Elsevier B.V. All rights reserved.
doi:10.1016/j.jallcom.2011.06.087

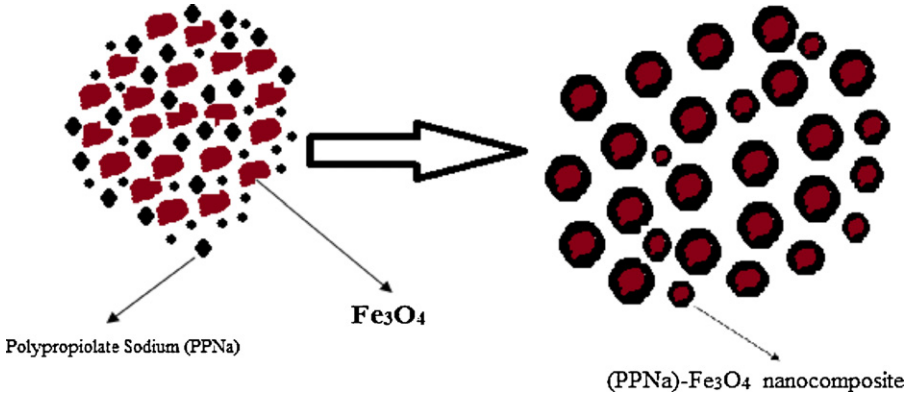

Scheme. Schematic representation of formation of PPNa–Fe_3O_4 nanocomposite.

2. Experimental

2.1. Chemicals

$FeCl_3 \cdot 6H_2O$ (99%), $FeCl_2 \cdot 4H_2O$ (99%) were purchased from Merck, propiolic acid, 96% was purchased from Aldrich and used without further purification. Catalyst, $[Rh(nbd)_2BF_4]$ (nbd, norbornadiene), was obtained from Alfa Aesar and used as received.

2.2. Instrumentation

X-ray powder diffraction (XRD) analysis was conducted on a Rigaku Smart Lab operated at 40 kV and 35 mA using Cu K_α radiation.

Fourier transform infrared (FT-IR) spectra were recorded in transmission mode with a Perkin Elmer BX FT-IR infrared spectrometer. The powder samples were ground with KBr and compressed into a pellet. FT-IR spectra in the range 4000–400 cm^{-1}.

Transmission electron microscopy (TEM) analysis was performed using FEI Tecnai G2 Sphera microscope. A drop of diluted sample in alcohol was dripped on a TEM grid and dried prior to insertion to TEM column.

The thermal stability was determined by thermo gravimetric analysis (TGA), Perkin Elmer Instruments model, STA 6000. The TGA thermograms were recorded for 5 mg of powder sample at a heating rate of 10°C/min in the temperature range of 30–800 °C under nitrogen atmosphere.

Magnetic measurements were performed by using a Quantum Design Vibrating sample magnetometer (QD-VSM). The sample was measured between ±10 kOe at room temperature (25 °C).

The electrical conductivity of the PPNa–Fe_3O_4 nanocomposite was studied in the temperature range of 20–120 °C with a heating rate of 10 °C/s. The sample was used in the form of circular pellets of 13 mm diameter and 3 mm thickness. The pellets (both nanocomposite and pristine) were sandwiched between gold electrodes and the conductivities were measured using Novocontrol dielectric impedance analyzer in the frequency range 1 Hz–3 MHz, respectively. The temperature (between −100 and 250 °C) was controlled with a Novocool Cryosystem.

^1H NMR and ^{13}C NMR were recorded using Bruker Ultra Shield Plus, Ultra long hold time 400 MHz NMR spectrometer.

2.3. Procedure

2.3.1. Synthesis of PPNa–Fe_3O_4 nanocomposite

To an aqueous solution of a mixture of Fe(III) and Fe(II) salts, in the molar ratio 2Fe(III):1Fe(II) was added and kept at a constant temperature of 40 °C for 15 min under vigorous stirring. Then a certain amount of PPNa and solution of sodium hydroxide was added till the pH was raised to 11 at which a black suspension was formed. This suspension was then refluxed at 80 °C for 6 h, under vigorous stirring and Ar gas. PPNa–Fe_3O_4 nanocomposite was separated from the aqueous solution by magnetic decantation, washed with distilled water several times and then dried in an oven overnight (Scheme).

3. Results and discussion

3.1. XRD analysis

Phase investigation of the crystalline product was performed by XRD and the diffraction pattern is presented in Fig. 1. The XRD pattern indicates that the product consists of magnetite, Fe_3O_4, and the diffraction peaks are broadened owing to very small crystallite size. All of the observed diffraction peaks are indexed by the cubic structure of Fe_3O_4 (JCPDS no. 19-629) revealing a high phase purity of magnetite. The following reaction was suggested for the formation of magnetite [11]:

$$Fe^{2+}{}_{(aq)} + 2Fe^{3+}{}_{(aq)} + 8OH^-{}_{(aq)} \rightarrow Fe_3O_{4(s)} + 4H_2O \quad (1)$$

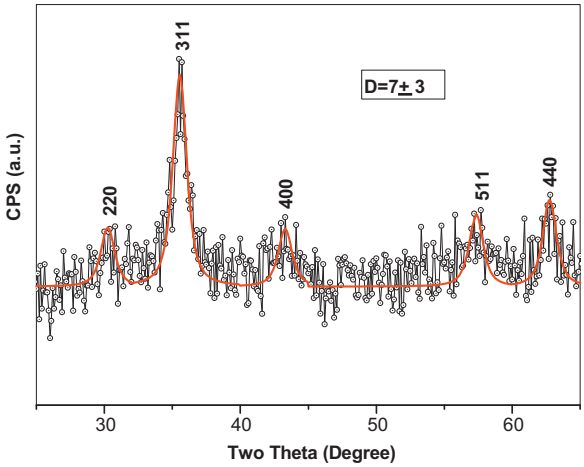

Fig. 1. XRD powder pattern and line profile fitting of PPNa–Fe_3O_4 nanocomposite.

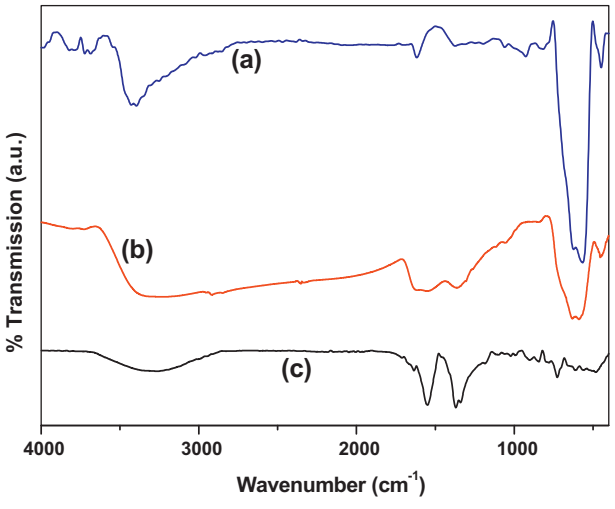

Fig. 2. FT-IR spectra of (a) uncoated Fe_3O_4 NP's, (b) PPNa–Fe_3O_4 nanocomposite, (c) PPNa.

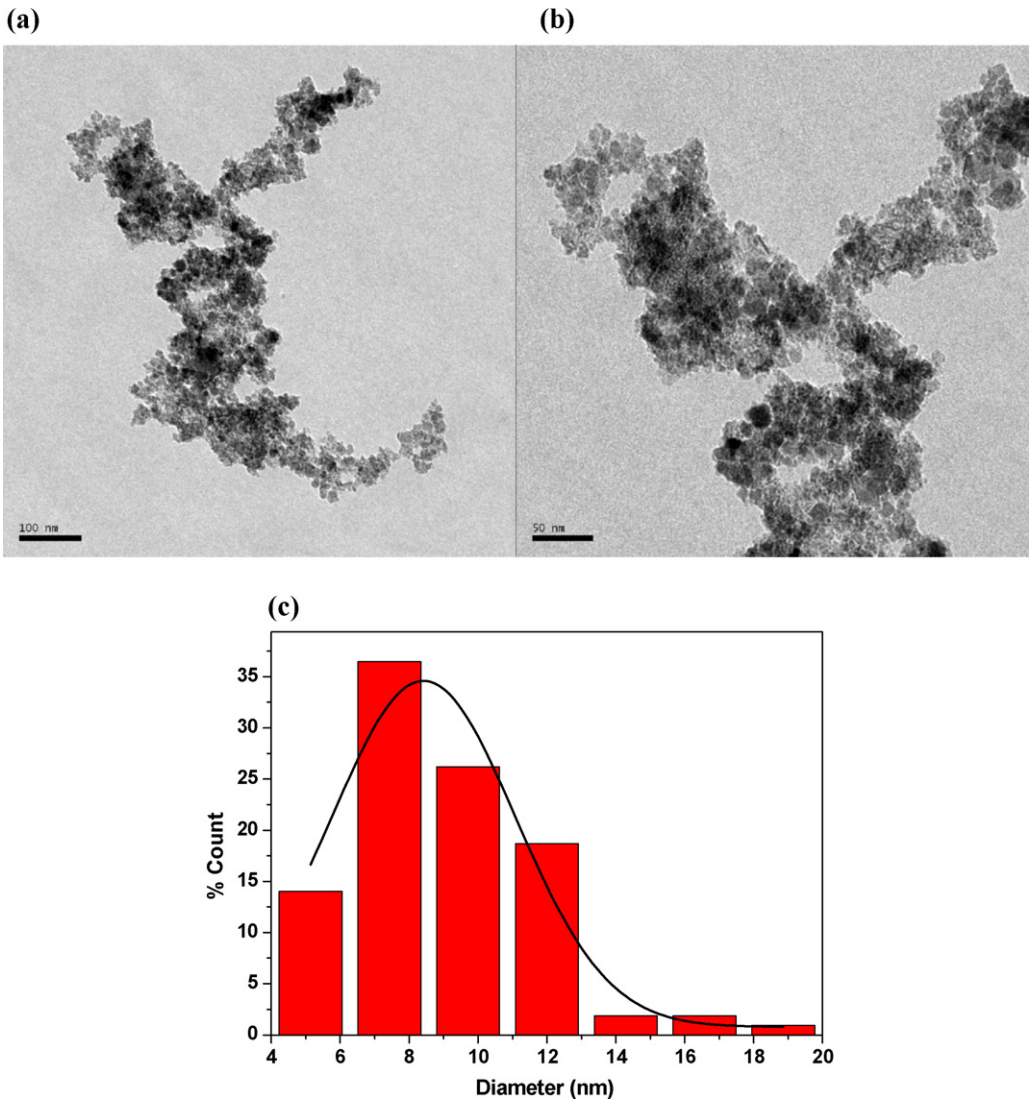

Fig. 3. (a, b) TEM micrographs of PPNa–Fe_3O_4 nanocomposite at different magnifications, (c) calculated histogram from several TEM images with log-normal fitting.

The mean size of the crystallites was estimated from the diffraction pattern by line profile fitting method using Eq. (1) given in Refs. [12,13]. The line profile, shown in Fig. 1 was fitted for observed five peaks with the following miller indices: (2 2 0), (3 1 1), (4 0 0), (5 1 1), (4 4 0). The average crystallite size, D and σ, was obtained as 7 ± 3 nm as a result of this line profile fitting [12,13].

3.2. FT-IR analysis

FT-IR spectra of Fe_3O_4 NP's, PPNa, PPNa–Fe_3O_4 and suggested linkage of PPNa to Fe_3O_4 surface are given in Fig. 2a–c, respectively. In the IR spectrum of polymer PPNa Fig. 2c, the large peak at 1557 cm^{-1} can be assigned to overlapped of C=O and C=C stretching. The peak at 1342 cm^{-1} belong to symmetric C–C bonding vibrations. And specific C–H out of plain deformation absorption signal at 726 cm^{-1} showed the cis conformation of this polymer. Also the broad O–H peak at 3315 cm^{-1} showed the presence of H_2O due to the hydration of the polymer [14,15].

The presence of the iron oxide nanoparticles evidenced by the strong absorbtion bands at around 570–590 cm^{-1} that confirm the metal–oxygen streching are present in Fig. 2a [16,17]. The absorption bands of asymmetric and symmetric stretching vibrations of CH_2 groups at 2918 cm^{-1} and 2850 cm^{-1} are well seen from Fig. 2c.

By comparing the separation of the symmetric and asymmetric stretching frequencies of the carboxylate ion ($\Delta\nu$) bound to transition metals with the separation measured for the corresponding sodium salt. According to Kirman et al. [18], if there is no C=O character in the spectrum and $\Delta\nu_{adsorbed}$ is similar to $\Delta\nu_{salt}$ then the adsorbed structure bidentate bridging. In our case, $\Delta\nu_{adsorbed}$ is ~180 cm^{-1} (1557–1373) and $\Delta\nu_{salt}$ is ~184 cm^{-1} (1553–1369).

3.3. TEM analysis

The TEM images and calculated histogram from several TEM images with log-normal fitting of the typical sample is shown in Fig. 3. Average particle size calculated by log-normal fitting to the size distribution histogram, was obtained as 9 ± 1 nm. As compared with the crystallite size obtained from X-ray line profile fitting, this reflects nearly single crystalline nature of the PPNa–Fe_3O_4 nanocomposite. It can be seen that the Fe_3O_4 NP's consist of spherical particles several nanometers long, which agreed well with the result from XRD. Parts of small particles have aggregated because of their extremely small size and high surface energies.

3.4. Thermal analysis

Thermal gravimetric analysis of Fe_3O_4 NP's, PPNa and PPNa–Fe_3O_4 nanocomposite was performed to investigate the stability of composite and to confirm the interaction between Fe_3O_4 nanoparticles and PPNa. No considerable weight loss was observed for Fe_3O_4 NP's (Fig. 4a). PPNa exhibits in three steps decomposition; the first one around between 50 °C and 150 °C due to the removal of adsorbed water with ~15% wt loss. The second step decomposition starts from ~200 °C and goes up to 750 °C (inset DTG graph) with about 50% loss (Fig. 4c). The third step decomposition of PPNa which was not complete in the working temperature.

Thermogram of PPNa–Fe_3O_4 nanocomposite is shown in Fig. 4b with a significant weight loss between the temperature 50 °C and 650 °C (inset graph). The weight loss is about 20% due to combustion of polymer in the structure of nanocomposite. TGA analysis showed the presence of 20% PPNa around 80% magnetic core (Fe_3O_4).

3.5. Magnetization

Magnetic characterization of bulk and PPNa coated Fe_3O_4 has been done by measuring M–H Hysteresis curves up to 1.5 T at room temperature and shown in Fig. 5. Both, bulk and the composite have immeasurable coercivity and remanence. In addition, magnetization of product increases with external magnetic field without reaching to a saturation even at 1.5 T. These are characteristic features of the superparamagnetic (SP) nanoparticles. Saturation magnetization of the samples is calculated using M vs. $1/H$ (M at $1/H \geq 0$) plots as 26 and 64 emu/g for the composite and bulk material, respectively. However, magnetization of the composite should be normalized to the weight of the magnetic core which is about 80% of the total weight. Then, M_s of the composite becomes 32.5 emu/g which is still very low compared to that of the bulk sample (64 emu/g). It should be noted that even saturation magnetization of the bulk sample is far from the theoretically predicted value (i.e., 92 emu/g). However, reduced magnetization is frequently observed in the SP magnetite particles and cannot be avoided when particle size is smaller than some threshold [19–23]. It can be explained by spin canting and presence of disordered spins at the surface [20–24]. As particle size decreases, effect of surface spins to the overall magnetization increases due to the presence of a considerably high fraction (nearly half) of all spins on the surface [25]. In the case of nanocomposite sample, this sharp decrease in M_s, from 64 to 32.5 emu/g, is due to the adsorption of surfactant molecules to the surface of magnetite. In our previous works [22,23,26,27] and in this study also, we have observed that surfactant molecules are bound to the surface of magnetite over oxygen atoms which cause pinning of some magnetic moments near surface. This weakens the super exchange interaction between Fe–O–Fe atoms. In this way, overall magnetization of the composite decrease further.

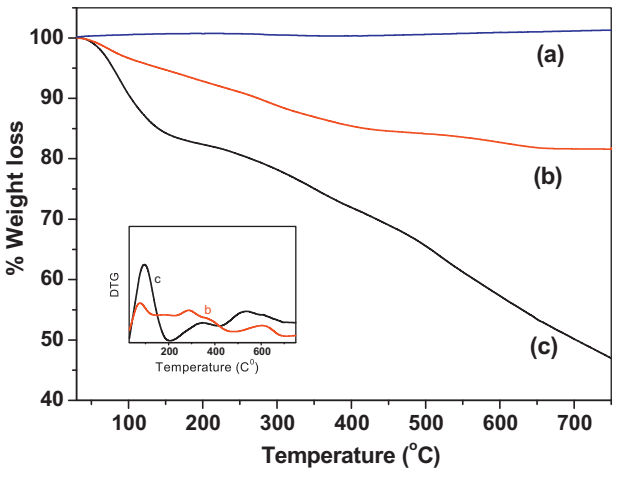

Fig. 4. TGA thermograms of (a) uncoated Fe_3O_4 NP's, (b) PPNa–Fe_3O_4 nanocomposite, (c) PPNa and DTG (inset).

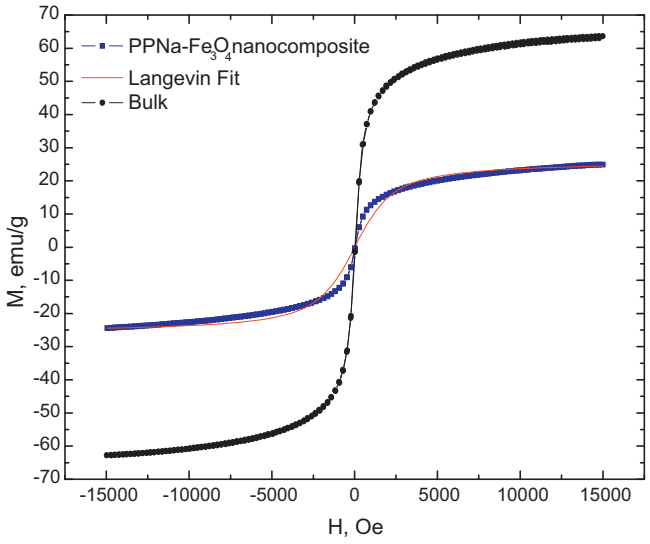

Fig. 5. M vs. H curves at room temperature and their log-normal size weighted Langevien fit of PPNa–Fe_3O_4 nanocomposite.

The average particle size of the SP particles can be calculated using room temperature hysteresis curves which are described by the Langevin function. Mean magnetic moment (μ) of particles can be determined by making theoretical fitting of this function to the magnetization curves as in Fig. 5. And, mean magnetic moment can be expressed in terms of Ms, particle size (D) and density of magnetite ($\rho = 5.18$ g/cm^3) as follows; $\mu = M_s \pi \rho D^3/6$. Thus, one can calculate particle size by inserting experimentally measured M_s and μ found from theoretical fitting. We have determined the mean magnetic moments composite as $4970\mu_B$ and average particles size as 8.2 ± 2 nm which agrees with the particle size determined from TEM micrographs and XRD patterns within the given uncertainities.

3.6. Temperature and frequency dependent conductivity and dielectric permittivity measurements

3.6.1. a.c. conductivity

The a.c. conductivities, $\sigma_{a.c.}(\omega)$ of both polypropiolate sodium (PPNa) polymer and polypropiolate sodium (PPNa)–Fe_3O_4 nanocomposite have been measured from 20 °C up to 120 °C using our impedance spectroscopy. Frequency-dependency of the conductivity, $\sigma_{a.c.}(\omega)$, has been measured using the following standard equation [28];

$$\sigma'(\omega) = \sigma_{ac}(\omega) = \epsilon''(\omega)\omega\varepsilon_0$$

where $\sigma'(\omega)$ is the real part of conductivity, ω is the angular frequency of the signal applied across the samples, ϵ'' is the imaginary part of complex dielectric permittivity (ϵ^*) and ε_0 ($= 8.852 \times 10^{-14}$ F/cm) is the vacuum permittivity.

The a.c. conductivities of both polypropiolate sodium (PPNa) polymer and polypropiolate sodium (PPNa)–Fe_3O_4 nanocomposite as a function of angular frequency for temperatures ranging from RT to 120 °C is illustrated in Fig. 6(a) and (b), respectively. In PPNa polymer case, a.c. conductivity is increased with a rule of $\sigma\alpha\omega^n$ while it depends strongly on both temperature and frequency. Value of the power exponent 'n' can vary differently with the attitude of

the conductivity at low and high frequency ranges of a transition region of 1 MHz. Other important characteristic behavior is that a.c. conductivity increases significantly at low and medium frequency while it depends less at high frequency over 1 MHz. At medium frequency, some wavy characteristic behavior of the conductivity can be seen shifted to the higher frequency region while temperature is elevated up to 80 °C. Then it is disappeared and obeys the power law characterization. When polypropiolate sodium (PPNa)–Fe_3O_4 nanocomposite is examined, initially, a.c. conductivity remains almost unchanged in the log–log scale up to 100 Hz at low temperature. Once the temperature is increased, its constant value at the log–log scale is shifted to higher frequency up to 1 MHz at 120 °C as shown with a row in Fig. 6(b). The rest is obeyed to the rule of power law of $\sigma\alpha\omega^n$.

As can be seen from Fig. 6(b), the curves of a.c. conductivity versus angular frequency for various temperatures comprise conductivity plateau regions in general. Additionally, the well-developed plateau region for the nanocomposites is shifted regularly to higher frequency region. After critical region of each a.c. conductivity–frequency dependencies, it obeys the well-known law of conductivity as described $\sigma(\omega, T) = \sigma(0, T) \cdot \omega^{n(T)}$. The higher frequency shifting of transition region is found to be linear as depicted in the log–log graph of the figure mentioned above. It can be pointed out that temperature dependency of the nanostructural

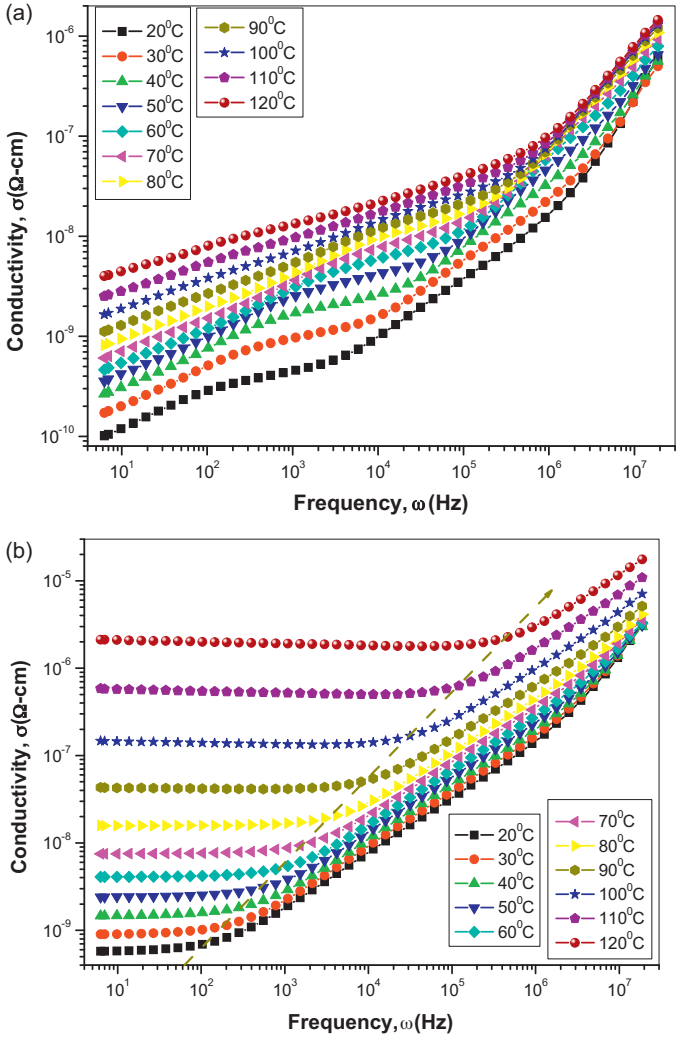

Fig. 6. a.c. conductivity of (a) PPNa, (b) PPNa–Fe_3O_4 nanocomposites as a function of angular frequency for a temperature range of 20 °C up to 120 °C.

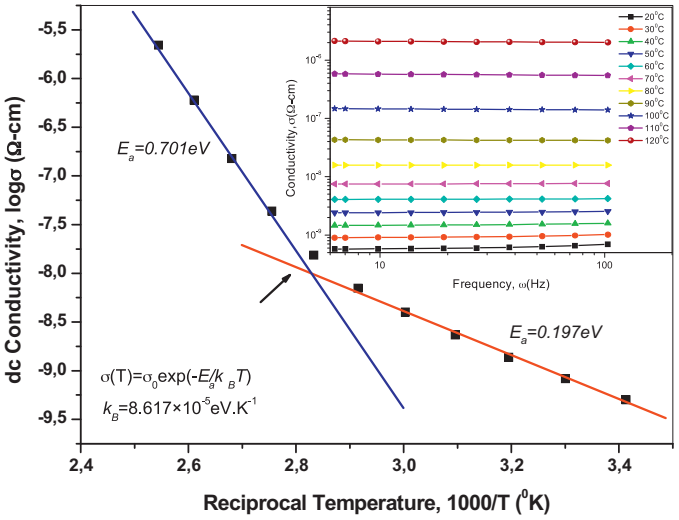

Fig. 7. d.c. conductivity of PPNa–Fe_3O_4 nanocomposites as a function of reciprocal temperature.

delocalisation of PPNa–Fe_3O_4 nanocomposites is crucial and reorganization process continues while the temperature increases. At the end of the treatment, a.c. conductivity becomes less dependent to angular frequency below 3×10^5 Hz at a higher temperature of 120 °C while at room temperature this type of dependency becomes short-ranged in frequency. This behavior can be attributed to the degree of the ferrite quantum dots coverage with the polymer PPNA according to temperature influence just before the conductivity power law obeys.

3.6.2. d.c. conductivity

The d.c. conductivity of PPNa–Fe_3O_4 nanocomposites as a function of reciprocal temperature is depicted in Fig. 7. As expected from our previous experiences, there exist two types of activation energies of 0.701 eV and 0.197 eV at low and high temperature ranges, respectively. Accordingly, the d.c. conductivity can be expressed as

$$\sigma(T) = \sigma_0 \exp\left(\frac{-E_a}{k_B T}\right)$$

As can be seen from the a.c. conductivity of both PPNa polymers and PPNa–Fe_3O_4 nanocomposites at low frequency region conductivity is found to be strongly temperature dependent while at high frequency region represent less frequency-dependency. This shows that capacitive effect is more prevailing, especially for PPNa–Fe_3O_4 nanocomposites. Its a.c. conductivity is found to obey the exponent function of angular frequency formulated as $\sigma(\omega, T) = \sigma(0, T) \cdot \omega^{n(T)}$ where each power exponent, $n(T)$, of both the low and high frequency regions is the temperature-dependent in a different manner [29].

The characteristic distinction of d.c. conductivity of the PPNa–Fe_3O_4 nanocomposites has been demonstrated in Fig. 7 with the illustration of linear fittings and transition regions. The conductivity curve demonstrates that d.c. conductivity strongly depends on temperature together with a transition region. Generally, PPNa polymer type-capped systems exhibit Arrhenius behavior at various temperature range, providing activation energy values below and above the transition region of a width of 20 °C in a measured temperature range of around 120 °C. The conductivity isotherm at low and high temperature can be fitted with Arrhenius equation as follows [30]; $\sigma_{dc} = \sigma_0 \exp(-E_a/k_B T)$ with different activation energies of $E_a = 0.197$ eV at lower temperature and 0.701 eV at higher temperatures, respectively. So, there would be two activation energies before and after transition temperature region of 80 °C. Where

σ_0 and E_a are the pre-exponential terms, and the activation energy for each region, respectively, and k_B (= 8.617385 × 10^{-5} eV/K) is the Boltzmann constant.

It is clearly found that electrical conductivity is strongly dependent on temperature. So d.c. conductivity of the PPNa-capped magnetite nanocomposites as in the case of both salicylic acid–Fe_3O_4 [31] and poly(2-thiophen-3-yl-malonic acid)–Fe_3O_4 [32] nanocomposite applications can be classified into three regions over a limited temperature range from RT up to approximately 150 °C. While general transition region of temperatures between 45 °C and 95 °C shows a metallic-like behavior, in this case at around 80 °C, which means electrical conductivity decreases with increasing temperature, d.c. electrical conductivity increases with increasing temperature with the formulation of $\log\sigma_{d.c.}$ versus $1/T$ before and after this region. Accordingly, this semiconducting phase in conductivity obeys Mott's variable range hopping mechanism of the conduction because the conduction mechanism of the nanocomposites shows a crossover from the Mott's law, $\exp(-AT^{1/4})$ [33,34], to a simply activated law, $\exp(-\Delta E/k_BT)$. This dependence can be often conveyed in the transition region (between 60 °C and 90 °C) as a slope in logarithmic conductivity versus reciprocal temperature graphs. So this behavior is attributed to the temperature-induced transition from 3D, to thermally activated behavior [35], where the physical meaning of the one fourth exponent in Mott's law can be ascribed to the reciprocal of the effective dimensionality of four (three spatial plus one energy) [36]. Here it should be emphasized that due to ferrites' semiconducting nature, the conductivity increases with increasing temperature.

3.6.3. Permittivity

The impedance measurements of the complex dielectric permittivity of the real ε' and imaginary ε'' parts of PPNa–Fe_3O_4 nanocomposites were examined and the real part of permittivity as a function of frequency at various temperatures is shown in Figs. 8 and 9(b) while those of PPNa polymers were illustrated in Figs. 8(a) and 9(a), respectively. In general, the real part of permittivity of the nanocomposites studied at higher temperature decreases sharply with increasing frequency at lower frequency range while at higher temperatures the decline in real part is very slow and also the actual intensity at this temperature range is quite low. This is an expected result because of reorganization of nanocomposite at high temperature range as a whole and phase transition when passed through the medium temperature range. At higher temperatures the variation of the real part of permittivity can be found to be less important to some extent in applying external electric field with higher frequency. Similar attitude could be seen in the PPNa polymer form. However, at higher frequency region real part of permittivity becomes less temperature-dependent.

There are interesting differences in real parts of permittivity of both PPNa polymer and PPNa capped-ferrites nanocomposites that around an angular frequency of 200 Hz, there has been a plateau for all temperatures studied here while there is a smooth tendency in the PPNa polymers. Another differentiation has been occurred at an angular frequency, ω, of around 100 kHz. At lower frequency real parts were recorded to be sharp drop at higher temperatures while smooth variation was observed at lower temperature. In general real permittivity for both the polymer and its counterpart nanocomposites could be considered to obey $\varepsilon'(\omega, T) = \varepsilon'(0)\omega^{-n(T)}$ within some limited region of different power exponent $n(T)$ as shown in Fig. 9.

Imaginary part of dielectric permittivity of both PPNa polymers and its counterpart capped-Fe_3O_4 nanocomposites versus angular frequency for temperatures ranging from RT to 120 °C was studied concisely as shown in Figs. 6 and 4. From the fitting parameters, logarithmic imaginary part of the permittivity for both samples

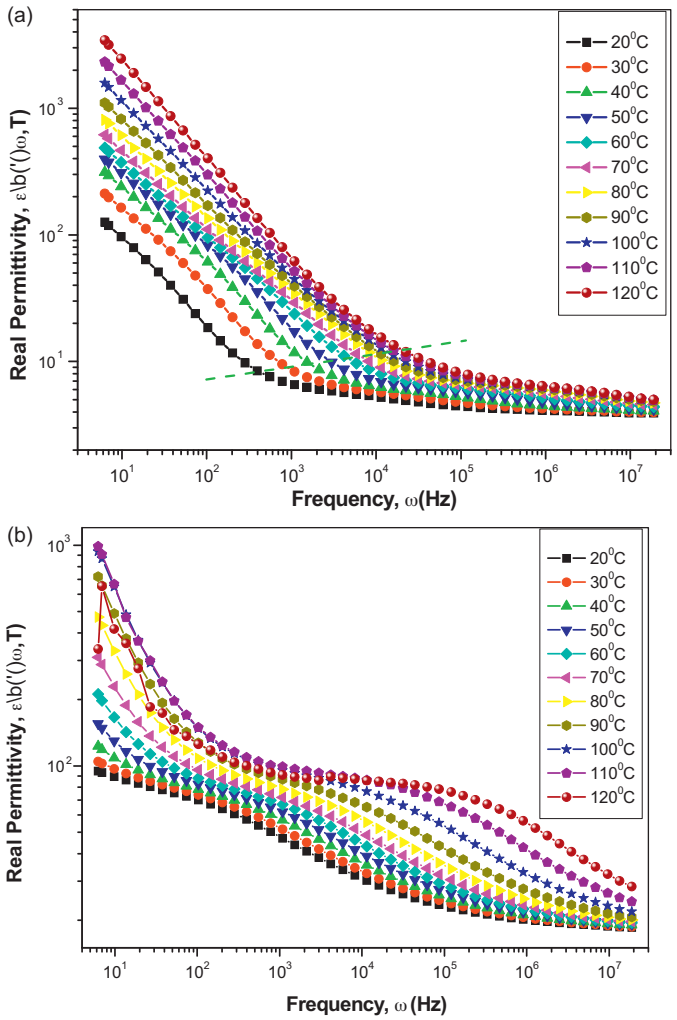

Fig. 8. Real permittivity of (a) PPNa, (b) PPNa–Fe_3O_4 nanocomposites as a function of angular frequency for a temperature range of 20 °C up to120 °C.

increases with temperatures while the exponent "n" is also found to vary with temperatures as shown in the relevant figure. Power exponent, n, is observed to be very regular, especially at lower frequencies. This attitude represents us that, on one hand, the capacitive response of the nanocomposites is highly dependent on temperature and furthermore, more dependent on the nature of the reorganization of the PPNa capped magnetite NPs. On the other hand, imaginary part is found to be dependent on reciprocal angular frequency $\varepsilon''(\omega, T) = \varepsilon''(0)\omega^{-n(T)}$ of applied signal. Within the frequency range of measurements the imaginary parts of the effective permittivity of nanocomposites exhibit spectra which can be analytically well represented by power laws. The associated power law exponents of imaginary parts of the permittivity, are well-developed in good agreement with data earlier reported [21].

Consequently, the dielectric constant increases usually with increasing temperature as seen in semiconducting materials. In some cases, the thermal energy converts the bound charges into the charge carriers, and intensifying charge carrier concentration always provides easy alignment of dipoles in the applied a.c. electrical field and accordingly increases in dielectric constants. Furthermore, the mobility of the charge carriers increases by increasing the temperature because of the building up in thermal energy.

More additionally, the temperature dependency of the nanostructural delocalization of PPNa–Fe_3O_4 nanocomposites has an

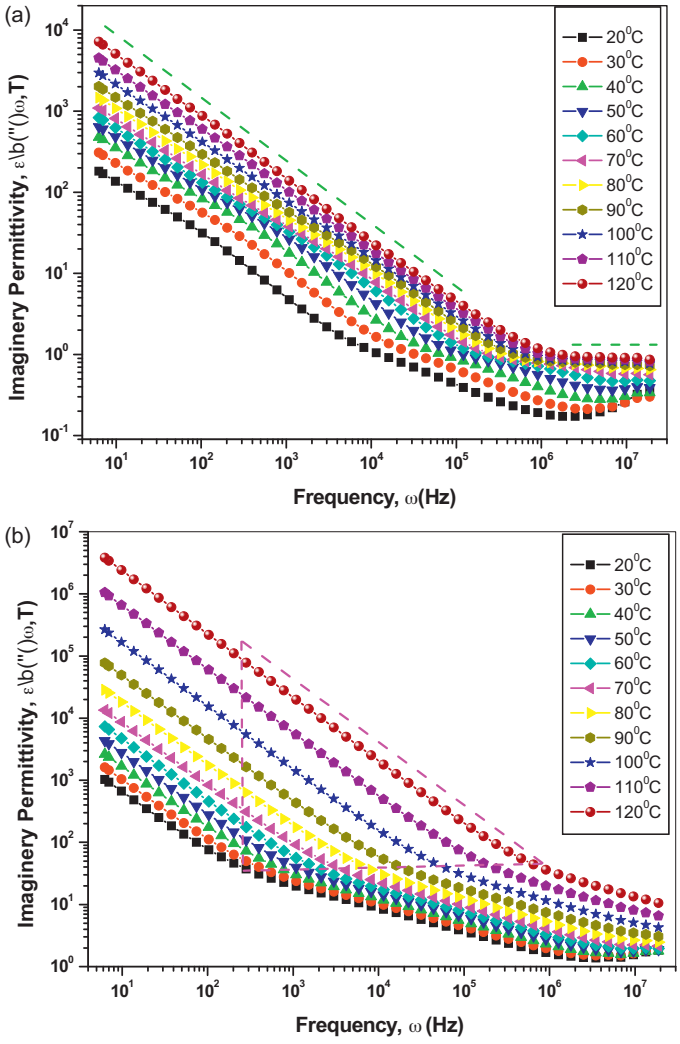

Fig. 9. Imaginary permittivity of (a) PPNa, (b) PPNa–Fe_3O_4 nanocomposites as a function of angular frequency for a temperature range of 20 °C up to120 °C.

influence on both conductivity and permittivity, and reorganization evolution continues while the temperature increases.

4. Conclusion

We have successfully polypropiolate sodium (PPNa)–Fe_3O_4 nanocomposite and characterized it in detail for composition, microstructure, a.c.–d.c. conductivity performance, and dielectric permittivity. PPNa is assessed to be covalently bonded to the Fe_3O_4 NP's surface. The magnetic core size of superparamagnetic PPNa–Fe_3O_4 nanocomposite was found slightly smaller than the size obtained from TEM, which reveals a core–shell type of structure due to the magnetically dead layer. The reduced saturation magnetization of the nanocomposite was explained by spin canting. It is pointed out that the a.c. conductivity of the nanocomposite studied here obeys the well-known conductivity power law as functions of frequency in which its characteristic temperature dependency also varies with the applied frequency range, say, high variations at lower frequency range while less sensitive at higher range. Moreover, the characterization of d.c. conductivity has shown two operating regions of the activation energy of 0.197 eV at lower temperature, and of 0.701 eV at higher temperature though reorganization process of nanocomposites took place at higher temperature. It has been discussed that the temperature dependency of both conductivity and permittivity has a crucial indication in the nanostructural delocalization of PPNa–Fe_3O_4 nanocomposites, and reorganization evolution continues while the temperature increases. Both real and imaginary parts of the permittivity studied here exhibit almost the same attitude which is the indication of the same capacity as in both energy storage, and energy dissipation within the PPNa and PPNa-capped ferrite nanocomposites.

Acknowledgements

The authors are thankful to the Fatih University, Research Project Foundation (Contract no: P50020902-2) and TUBITAK (Contract no:110T487) for financial support of this study.

Appendix A. Supplementary data

Supplementary data associated with this article can be found, in the online version, at doi:10.1016/j.jallcom.2011.06.087.

References

[1] Æ. Wei Wu, Æ. Quanguo He, Changzhong Jiang, Nanoscale Res. Lett. 3 (2008) 397.
[2] D. Patel, J.Y. Moon, Y. Chang, T.J. Kim, G.H. Lee, Colloids Surf. A 91 (2008) 313.
[3] Z. Durmus, H. Kavas, A. Baykal, H. Sozeri, L. Alpsoy, S.Ü. Celik, M.S. Toprak, J. Alloy Compd. 509 (2011) 2555.
[4] S. Mørup, M.F. Hansen, C. Frandsen, Comprehensive Nanosci. Technol. 1 (14) (2011) 437.
[5] M.Z. Kassaee, Hassan Masrouri, Farnaz Movahedi, Appl. Catal. A: Gen. 395 (2011) 28.
[6] Y. Jun, J. Choi, J. Cheon., Chem. Commun. (2007) 1203.
[7] K. Singh, A. Ohlan, A.K. Bakhshia, S.K. Dhawan, Mater. Chem. Phys. 119 (2010) 201.
[8] M. Aydın, Z. Durmus, H. Kavas, B. Esat, H. Sözeri, A. Baykal, F. Yılmaz, M.S. Toprak, Polyhedron 30 (2011) 1120.
[9] Y. Li, G. Chen, Q. Li, G. Qiu, X. Liu, J. Alloy Compd. 509 (2011) 4104.
[10] W. Wu, Q. He, C. Jiang, Nanoscale Res. Lett. 3 (2008) 397.
[11] Z. Durmus, H. Kavas, M.S. Toprak, A. Baykal, T.G. Altıncekic, A. Aslan, A. Bozkurt, S. Cosgun, J. Alloy Compd. 484 (2009) 371, 434.
[12] T. Wejrzanowski, R. Pielaszek, A. Opalińska, H. Matysiak, W. Lojkowski, K.J. Kurzydlowski, Appl. Surf. Sci. 253 (2006) 204.
[13] R. Pielaszek, Appl. Crystallography Proceedings of the XIX Conference, vol. 43, Krakow Poland, 2003.
[14] I.A. Badmaeva, N.V. Surovtsev, V.K. Malinovskii, L.L. Sveshnikova, J. Struct. Chem. 51 (2010) 244.
[15] K. Maeda, H. Goto, E. Yashima, Macromolecules 34 (2001) 1160.
[16] Z. Durmus, Master Thesis, Fatih Univ., Istanbul, Turkey, (2009) 443.
[17] T. Ozkaya, M.S. Toprak, A. Baykal, H. Kavas, Y. Koseoglu, B. Aktas, J. Alloy Compd. 18 (2009) 444.
[18] L.J. Kirman, P.D. Fawell, W.V. Bronswijk, Langmuir 19 (2003) 5802.
[19] J. Mürbe, A. Rechtenbach, T. Töpfer, Mater. Chem. Phys. 110 (2008) 426.
[20] R.H. Kodama, A.E. Berkowitz, E.J. McNiff Jr., S. Foner, Phys. Rev. Lett. 77 (1996) 394.
[21] X. Batlle, A. Labarta, J. Phys. D: Appl. Phys. 35 (2002) R15.
[22] Z. Durmus, H. Erdemi, A. Aslan, M.S. Toprak, H. Sozeri, A. Baykal, Polyhedron 30 (2011) 419.
[23] B. Ünal, Z. Durmus, A. Baykal, H. Sözeri, M.S. Toprak, L. Alpsoy, J. Alloy Compd. 505 (2010) 172.
[24] A.E. Berkowitz, J.A. Lahut, I.S. Jacobs, L.M. Levinson, D.W. Forester, Phys. Rev. Lett. 34 (1975) 594.
[25] C. Kittel, Introduction to Solid State Physics, Wiley, New York, 1971.
[26] Z. Durmus, H. Sozeri, B. Unal, A. Baykal, R. Topkaya, S. Kazan, M.S. Toprak, Polyhedron 30 (2011) 322.
[27] K. Uzun, E. Cevik, M. Senel, H. Sozeri, A. Baykal, M.F. Abasıyanık, M.S. Toprak, J. Nanopart. Res. doi:10.1007/s11051-010-9902-9.
[28] S.U. Celik, A. Bozkurt, Eur. Polym. J. 44 (2008) 213.
[29] Z. Durmus, B. Unal, M.S. Toprak, A. Aslan, A. Baykal, Physica B 406 (2011) 2298.
[30] N.F. Mott, Philos. Mag. 19 (1969) 835.
[31] B. Unal, Z. Durmus, H. Kavas, A. Baykal, M.S. Toprak, Mater. Chem. Phys. 123 (2010) 184.
[32] E. Karaoğlu, A. Baykal, H. Deligöz, M. Şenel, H. Sözeri, M.S. Toprak, J.Alloy Compd. doi:10.1016/j.jallcom.2011.06.002.
[33] R. Zallen, The Physics of Amorphous Solids, Wiley–Interscience, NewYork, USA, 1998.
[34] M. Okutan, H.I. Bakan, K. Korkmaz, F. Yakuphanoglu, Phys. B: Condens. Matter. 355 (1–4) (2005) 176.
[35] D. Jana, J. Fort, Physica B 344 (2004) 62.
[36] C. Brosseau, P. Talbot, IEEE Trans. Dielectr. Electr. Insul. 11 (5) (2004) 819.